JOTA manuscript No.
(will be inserted by the editor)

On the Minimum-time Control Problem for Differential Drive Robots with Bearing Constraints

Andrea Cristofaro · Paolo Salaris · Lucia Pallottino · Fabio Giannoni · Antonio Bicchi

Received: date / Accepted: date

Communicated by: Felix L. Chernousko

Andrea Cristofaro (Corresponding author), Fabio Giannoni

School of Science and Technology, University of Camerino

Via Madonna delle Carceri 9, 62032 Camerino MC, Italy.

{andrea.cristofaro,fabio.giannoni}@unicam.it

Andrea Cristofaro is also with the Department of Engineering Cybernetics, NTNU,

O.S. Bragstads Plass 2D, 7491 Trondheim, Norway.

Paolo Salaris

Istitut National de Recherche en Informatique et en Automatique (INRIA)

2004, Route des Lucioles, 06902 Sophia Antipolis, France

paolo.salaris@inria.fr

Lucia Pallottino, Antonio Bicchi

Research Center "E. Piaggio" & Dipartimento di Ingegneria dell'Informazione,

University of Pisa, 1, Largo Lucio Lazzarino, 56122 Pisa, Italy

{lucia.pallottino, antonio.bicchi}@unipi.it

Antonio Bicchi is also with the Department of Advanced Robotics, Istituto Italiano

di Tecnologia, 30, via Morego, 16163 Genova, Italy

Abstract This paper presents a study of analysis of minimum time trajectories for a differential drive robot equipped with a fixed and limited Field-Of-View (FOV) camera, which must keep a given landmark in view during maneuvers. Previous works have considered the same physical problem and provided a complete analysis/synthesis for the problem of determining the shortest paths. The main difference in the two cost functions (length vs. time) lays on the rotation on the spot. Indeed, this maneuver has zero cost in terms of length and hence leads to a 2D shortest path synthesis. On the other hand, in case of minimum time, the synthesis depends also on the orientations of the vehicle. In other words, the not zero cost of the rotation on the spot maneuvers leads to a 3D minimum time synthesis. Moreover, the shortest paths have been obtained by exploiting the geometric properties of the extremal arcs, i.e. straight lines, rotations on the spot, logarithmic spirals and involute of circles. Conversely, in terms of time, even if the extremal arcs of the minimum-time control problem are exactly the same, the geometric properties of these arcs change, leading to a completely different analysis and characterization of optimal paths. In this paper, after proving the existence of optimal trajectories and showing the extremal arcs of the problem at hand, we provide the control laws that steer the vehicle along these arcs and the time-cost along each of them. Moreover, this being a crucial step toward numerical implementation, optimal trajectories are proved to be characterized by a finite number of switching points between different extremal arcs, i.e. the concatenations of

extremal arcs with infinitely many junction times are shown to violate the optimality conditions.

Keywords Time optimal paths · Nonholonomic dynamical systems · Bearing constraints · Differential-drive vehicles

Mathematics Subject Classification (2000) 34H05 · 37J60 · 49J15 · 93C85

1 Introduction

The interest of both academic and industrial communities in topics related to autonomous mobile robots has remarkably increased in the last decade, these being very suitable to be used in conditions and environments that are barely accessible for humans [1]. The most important issues in mobile robotics, which deeply influence the accomplishing of assigned tasks and hence the control laws, concern the directionality of motion (i.e. nonholonomic constraints) and limitation of sensory constraints (i.e. Field-Of-View (FOV)). Localization tasks, formation control and maintain visibility of some objects in the environment imply that some landmarks must be kept in sight and involve several interesting mathematical problems to be addressed [2–6]. Optimization problems are typically incorporated in the motion planning framework, i.e. the analysis and synthesis of prescribed trajectories to be followed by the robot [7–11]. Time optimal trajectories for a bounded velocity Differential Drive Robot (DDR), which moves on a unobstructed plane, have been derived in [12]. In particular, authors provided a proof of the existence and an analysis

of the structure of the time optimal trajectories. Moreover, they furnished an algorithm to determine all optimal trajectories with the associated time cost. If, in addition to the nonholonomic constraints, the robot is supposed to carry a fixed on-board camera with limited FOV, the problem becomes even more interesting and complex as the vision constraints further limit feasible maneuvers. This research aims at deriving the time optimal trajectories for a DDR from any starting configuration of the vehicle to a desired one, while keeping a given landmark in sight during maneuvers. We consider a pinhole camera model [13] with a limited horizontal and vertical angle of view (see Figure 1), whose principal axis forms and angle Γ w.r.t. the robot forward direction.

The FOV problem has been successfully solved for nonholonomic vehicle, e.g. in [14–16] where the resultant path is not optimal. An optimal solution for a nonholonomic vehicle with FOV constraints has been furnished in [17] and [18]. In particular, [17] provides the shortest paths synthesis in case of a camera modeled as a frontal and symmetric (w.r.t. the forward direction of motion), planar cone, i.e. only horizontal limits of the sensor are taken into account. In [18] shortest paths to generic FOVs, including side and lateral sensors (the forward direction of motion in not necessarily included inside the FOV) has been obtained. Moreover, in [19] and [20] authors also introduced the vertical constraint limits imposed by the camera: it is worth to note that in this case, the optimal solution may not exist for some particular initial/final robot configurations.

On the other hand, optimal trajectories for DDRs without FOV constraints are also derived in [21] where the total amount of wheel rotation is optimized, while in [22] time optimal trajectories are obtained for an omnidirectional vehicle. The methodology used in [12] is an extension of optimal control techniques developed in [11, 23, 24] for steered vehicles. Moreover, in [25] a geometric algorithm to derive time optimal trajectories for a bidirectional steered robot is developed. The study of optimal controls for such vehicles started with [26] and [10].

In the case of time-optimal paths for a DDR with limited FOV, some preliminary results are available in [27], where a characterization of the extremal paths for the system is derived and moreover a comparison of some concatenations of extremals is provided in order to reduce the complexity of the problem toward the definition of a sufficient set of optimal maneuvers.

As a major novel contribution to the problem, in this paper the existence of time optimal trajectories for a DDR with limited FOV is formally addressed, the expression of optimal controls is given and optimal paths are proved to consist of a finite number of maneuvers. As already mentioned, the existence of optimal solutions to control problems in the presence of nonholonomic and state/input constraints is a major problem and it needs to be carefully addressed [28–30]. Moreover, the demonstration that optimal trajectories are composed by a finite number of extremal concatenations is a non trivial result, important both from a theoretical perspective and for numerical approximations of optimal solutions.

The paper is structured as follows. The basic setup is given in Section 2, while Section 3 focuses on the Hamiltonian formulation for the constrained optimization problem. Section 4 addresses controllability and existence of optimal paths, and the characterization of time costs associated to extremal arcs is described in Section 5. Finally, the analysis of the junction times set, i.e. the set of time instants corresponding to switching between different externals, is carried out in Section 6. Some conclusions and a resume of future perspectives and open problems close the paper.

2 Problem Definition

In this section the kinematic model of a Differential Drive Robot (DDR) [12] will be introduced for reader convenience. The robot has an on-board camera with a limited Field-Of-View (FOV). The camera is represented as a rectangular right pyramid, which is a typical shape in case of pinhole camera model [31]. Finally, the constraints on the robot motion imposed by the camera in order to maintain a fixed landmark in the environment inside the limited FOV will be also introduced.

2.1 The Robot and the Camera Models

Let us consider a DDR moving on a plane where a right–handed reference frame $\langle W \rangle$ is defined with origin in O_w and axes X_w, Z_w. The configuration of the vehicle is described by $\xi(t) = (x(t), z(t), \theta(t))$, where $(x(t), z(t))$ is the position in $\langle W \rangle$ of a reference point in the vehicle, and $\theta(t)$ is the heading angle,

i.e. the vehicle heading with respect to the X_w axis (see Figure 1(a)). The vehicle velocities are subject to the nonholonomic constraint that, in Pfaffian form assumes the following form:

$$A(\xi)\dot{\xi} = \begin{bmatrix} \sin\theta & -\cos\theta & 0 \end{bmatrix} \begin{bmatrix} \dot{x} \\ \dot{z} \\ \dot{\theta} \end{bmatrix} = 0$$

It is important to note that without this nonholonomic constraint, the problem tackled in this paper becomes trivial even in case of FOV constraints that will be introduced in the next subsection. Indeed, this constraint limits instantaneous movements that are orthogonal to the heading direction as it occurs for cars and bicycle. However, the vehicle can reach any point on the motion plane by manoeuvring – the controllability property holds for the DDR. Feasible velocities for the DDR are hence contained in the null space of the constraint matrix $A(\xi)$

$$\mathcal{N}(A^T(\xi)) = \left\{ \begin{pmatrix} \cos\theta \\ \sin\theta \\ 0 \end{pmatrix}, \begin{pmatrix} 0 \\ 0 \\ 1 \end{pmatrix} \right\}.$$

Hence the kinematic model of the DDR in cartesian coordinates is given as

$$\dot{\xi} = \begin{bmatrix} \cos\theta \\ \sin\theta \\ 0 \end{bmatrix} v(t) + \begin{bmatrix} 0 \\ 0 \\ 1 \end{bmatrix} \omega(t)\,, \tag{1}$$

where $v(t)$ and $\omega(t)$, also known as pseudovelocities, are the driving (or forward) and the steering (or angular) velocities.

To simplify the analysis of the problem, referring to Figure 1(a) we choose polar coordinates instead of cartesian ones to represent the kinematic model of the DDR: $q(t) = [\rho(t)\ \psi(t)\ \beta(t)]^T$ with $\rho = \sqrt{x^2 + z^2}$, $\psi = \arctan\left(\frac{z}{x}\right)$ and $\beta = \arctan\left(\frac{z}{x}\right) - \theta + \pi$. The kinematic model of the DDR becomes

$$\dot{q} = g_1(q)v + g_2(q)\omega. \tag{2}$$

where

$$g_1(q) = \left[-\cos\beta\ \frac{\sin\beta}{\rho}\ \frac{\sin\beta}{\rho}\right]^T, \quad g_2(q) = [0\ 0\ -1]^T. \tag{3}$$

From a practical point of view, usually a DDR has two wheels, one on the right and one on the left, actuated by two motors whose control inputs are assumed to be their angular velocities. Denoting by w_R and w_L the angular velocities of the right and left wheel, respectively, we have

$$v = \frac{w_R + w_L}{2}, \quad \omega = \frac{w_R - w_L}{2b} \tag{4}$$

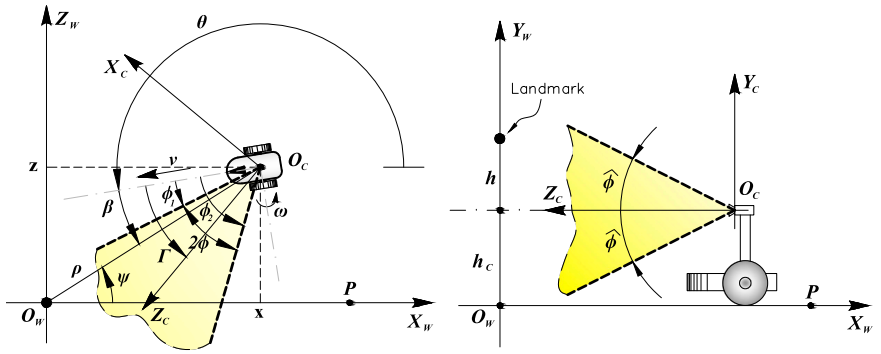

(a) Cartesian and polar coordinates of the robot and H-FOV constraints.

(b) V-FOV constraints. h is the height of the landmark w.r.t. the plane $X_c \times Z_c$.

Fig. 1 Mobile robot and systems coordinates. The robot's task is to reach point P from any initial position Q on the motion plane while keeping the landmark within a limited FOV (dashed lines).

where b is half of the wheels axle length. In the following, we will refer to v, ω or w_R and w_L as the pair of control inputs of the DDR. Referring to the equivalent input representation (4) we assume, without loss of generality, the bounds $w_i \in [-1,\, 1],\ i = L,\, R$.

The vehicle carries an on-board rigidly fixed pinhole camera with a reference frame $\langle C \rangle = \{O_c, X_c, Y_c, Z_c\}$ such that the optical center O_c corresponds to the robot's center $[x(t), z(t)]^T$ and the optical axis Z_c forms an angle Γ with the robot's forward direction (see Figure 1). Without loss of generality, we will assume $0 \leq \Gamma \leq \frac{\pi}{2}$, so that, when $\Gamma = 0$ the Z_c axis is aligned with the robot's forward direction, whereas, when $\Gamma = \frac{\pi}{2}$, the Z_c axis is perpendicular to the robot's forward direction. The camera has a limited Field-Of-View (FOV) represented as a rectangular right pyramid where $\hat{\phi}$ and ϕ are the half of the vertical and horizontal angular aperture of the camera, i.e. half of the apex angles which are the dihedral angles between the opposite side faces of the pyramid. We will refer to those angles as the vertical and horizontal angular aperture of the sensor, respectively. In the following, we consider the most interesting case in which $\hat{\phi}$ and ϕ are less than $\pi/2$. Let $\phi_1 = \Gamma - \phi$ and $\phi_2 = \Gamma + \phi$ be the angles between the robot's forward direction and the right and left sensor's border w.r.t. Z_c axis, respectively (see Figure 1(a)). Notice that, the known parameters ϕ, $\hat{\phi}$, Γ define a range of different possible camera FOVs and configurations between the robot and the camera. However, they are assumed to be fixed and do not change during the robot motion.

We assume that the feature to be kept within the on-board limited FOV sensor is placed on the axis through the origin O_w, perpendicular to the plane of motion, so that its projection on the motion plane coincides with the center O_w (see figure 1). The feature has height h from the plane $X_c \times Z_c$.

Referring to Figure 1(a), the horizontal FOV (H-FOV), with characteristic angle 2ϕ, generates the following constraints:

$$-\beta + \phi_1 \leq 0, \quad \beta - \phi_2 \leq 0\,. \tag{5}$$

while the vertical FOV (V-FOV), with characteristic angle $2\hat{\phi}$, generates the following one

$$\rho \cos(\beta - \Gamma) \geq \frac{h}{\tan\hat{\phi}} =: R_b \tag{6}$$

where R_b is a constant and represents the minimum distance from O_w that the vehicle can reach without violating the V-FOV constraints. Let C_b denote the circumference centered in the origin of radius R_b. The expression of constraint (6) is not straightforward; indeed we need to use the pinhole camera model to get it (see [20] for a detailed proof on how this constraint is obtained).

2.2 Optimal Control Problem Statement

The optimal control problem consists in determining, for any initial position of the system $Q = (\rho_Q, \psi_Q) \in \mathbb{R}^2$ on the plane $X_w \times Z_w$ with β_Q such that (5) and (6) are verified, the minimum time trajectory from Q to the robot target position $P = (\rho_P, \psi_P) \in \mathbb{R}^2$, $P \neq Q$ and with β_P subjects to the same

constraints of β_Q. In the following, without loss of generality, we will assume P to lay on the X_w axis, with $\psi_P = 0$ (see Figure 1).

For given and fixed parameters ϕ, $\hat{\phi}$, Γ and hence R_b, the state constraints (5)-(6) are imposed on the state variable of the system along the whole trajectory. This gives rise to the inclusion $q(t) \in \mathcal{S}$ where

$$\mathcal{S} := \{(\rho(t), \psi(t), \beta(t)) \in \mathbb{R}^3 : |\beta(t) - \Gamma| \leq \phi,\ \rho(t)\cos(\beta(t) - \Gamma) \geq R_b\}. \quad (7)$$

At the same time, limits on the pair (w_R, w_L)gives rise to the control domain $\mathcal{U} \ni (v, \omega)$ which turns out to be a diamond (see [25]), i.e.

$$\mathcal{U} = \{(v, \omega) \in \mathbb{R}^2 : 0 \leq |v| + b|\omega| \leq 1\}. \quad (8)$$

Summarising, the optimal control problem to be solved is

Problem 2.1 (Optimal control problem with pure state constraints) Let $q(t) = [\rho(t),\ \psi(t),\ \beta(t)]^T$ be the state of the nonlinear control-affine system whose dynamics are $\dot{q}(t) = g_1(q(t))v(t) + g_2(q(t))\omega(t)$ with $g_1(q)$, $g_2(q)$ given by (3) and control inputs ($v(t)$, $\omega(t)$). The optimal control problem is

$$\min_{v,\,\omega} \int_0^T L(q(t), v(t), \omega(t), t)\,\mathrm{d}t := \min_{v,\,\omega} \int_0^T 1\,\mathrm{d}t$$

subject to:

$(v,\ \omega) \in \mathcal{U}$

$Q = (\rho(0)\cos(\psi(0)), \rho(0)\sin(\psi(0)))$

$P = (\rho(T)\cos(\psi(T)), \rho(T)\sin(\psi(T))) := (\rho_P, 0)$

$q(t) \in \mathcal{S}\ \forall t \in [0, T]$

where Q is the initial position of the system, P is the target position of the system, v, ω are the inputs of the system, $\mathcal{U}$ is the set of admissible inputs given by (8) and $\mathcal{S}$ is the set of admissible states given by (7).

Before using the Pontryagin Maximum Principle (PMP) to characterize extremal arcs of the proposed optimal control problem, we first briefly report some useful geometric properties, obtained in [32], that can be exploited to simplify the analysis.

Remark 2.1. The H-FOV and the V-FOV constraints (5) and (6) can be simultaneously active only along a 1-dimensional curve C_S, which is a circumference centered in O_w with radius $\rho_S = \frac{R_b}{\cos\phi}$.

The above remark allows to consider separately the horizontal and vertical constraints; in particular, we can subdivide the motion plane in three distinct regions (see Figure 2)

$$Z_0 := \{(\rho, \psi) : \rho < R_b\}$$

$$Z_1 := \{(\rho, \psi) : R_b \leq \rho \leq \rho_S\}$$

$$Z_2 := \{(\rho, \psi) : \rho \geq \rho_S\}\,.$$

The disk Z_0 is the set of points in $\mathbb{R}^2$ that violates V–FOV constraint (6) for any value of β and hence is inaccessible. The annulus Z_1 is instead the set where the V–FOV constraint determines the optimal path behavior: in fact, as long as $q \in Z_1$ and the V–FOV constraint holds true, one has necessarily $|\beta - \Gamma| \leq \phi$ where the equality holds only on the boundary C_S. Finally, the unbounded region Z_2 does correspond to the set where the optimal path behavior is ruled by H–FOV constraints: indeed, as long as $q \in Z_2$ and both

the H–FOV holds true, one has necessary $\rho\cos(\beta - \Gamma) \geq R_b$, where again the equality holds only on the boundary C_S.

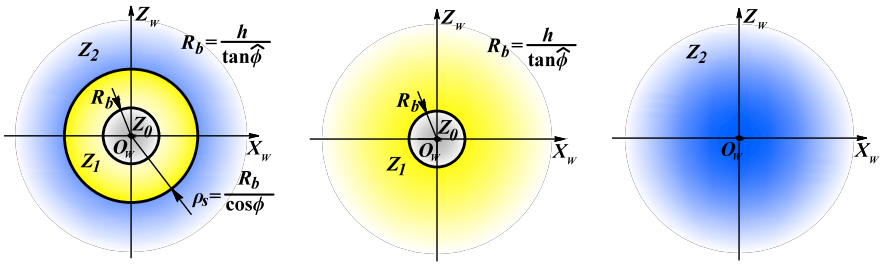

(a) Subdivision of the motion plane with both H-FOV and V-FOV constraints

(b) Motion plane in the case of V-FOV constraints only, as in [19]

(c) Motion plane in the case of H-FOV constraints only, as in [17]

Fig. 2 Subdivision of the motion plane according to Remark 2.1.

3 Adjoint Equations and Extremal Arcs

In order to characterize the extremal arcs and the associated control inputs, we now study the Hamiltonian function associated to the optimal control problem 2.1. The goal is to determine the necessary conditions for optimality by using the PMP. Both H-FOV and V-FOV constraints depend on the states $q(t)$ and not (explicitly) on the control variables $(v(t), \omega(t))$. There are two possibility to deal with pure state constraints (see [33] and references therein). In the first one, also known as direct adjoint approach, the pure state constraints are directly adjoined to the Hamiltonian pre-multiplied by suitable multipliers. In the second one, also known as indirect adjoint approach, the pure state constraints is derived w.r.t. the time along the trajectory of the dynamic system

until the control inputs appear (this is suggested by [34,35] for the first order state constraints, i.e. the control inputs appear after the first derivative of the constraints and then in [36,37] for higher order state constraints). We decide to adopt the indirect adjoint approach in this paper. Hence, given the pure state constraints (7), these can be easily rearranged as $s(q) \leq (0,\, 0,\, 0)^T$. The first order derivative $s^{(1)}(q,\, v,\, \omega)$, which is sufficient to reveal the inputs, is

$$s^{(1)}(q,\, v,\, \omega) = \begin{pmatrix} \frac{\sin\beta}{\rho} v - \omega \\ -\frac{\sin\beta}{\rho} v + \omega \\ \cos\Gamma v - \rho \sin(\beta - \Gamma)\omega \end{pmatrix}. \tag{9}$$

The constrained Hamiltonian of the system is hence given by

$$\begin{aligned} H(\rho, \psi, \beta, v, \omega) = 1 - \lambda_1 \cos\beta v + \lambda_2 \frac{\sin\beta}{\rho} v + \\ + (\lambda_3 - \mu_1 + \mu_2) \left(\frac{\sin\beta}{\rho} v - \omega \right) + \\ + \mu_3 (\cos\Gamma\ v - \rho \sin(\beta - \Gamma)\omega), \end{aligned} \tag{10}$$

with adjoints dynamics $\dot{\lambda} = -\frac{\partial H}{\partial q}$ and where the first derivative of the pure state constraints are added to the Hamiltonian pre-multiplied by nonnegative and nondecreasing multipliers on the boundary intervals of $s(q)$, i.e. $\mu_1, \mu_2,\, \mu_3 \geq 0$ and $\dot{\mu}_1, \dot{\mu}_2,\, \dot{\mu}_3 \leq 0$. Moreover, when $s_i(q) = 0$, it holds $s_i^{(1)}(q,\, v,\, \omega) = 0$ while $\mu_i = 0$ when $s_i(q) < 0$ for $i = 1,\, 2,\, 3$. To determine the necessary conditions of optimality [35,37] we study constrained and unconstrained arcs separately.

3.1 Unconstrained Arcs

Let us suppose that the initial condition $q(0)$ is such that $(\rho(0), \psi(0)) \in Z_1 \cup Z_2$ and

$$\phi_1 < \beta(0) < \phi_2, \quad \rho(0)\cos(\beta(0) - \Gamma) > R_b\,.$$

As a consequence, there always exists $t_1 > 0$ such that the constraints are not active for the interval $I_1 = [0, t_1[$. The adjoint equations reduce to

$$\begin{aligned}
\dot{\lambda}_1 &= (\lambda_2 + \lambda_3)\frac{\sin\beta}{\rho}v \\
\dot{\lambda}_2 &= 0 \\
\dot{\lambda}_3 &= \lambda_1 \sin\beta v + (\lambda_2 + \lambda_3)\frac{\cos\beta}{\rho}v.
\end{aligned}$$

The unconstrained Hamiltonian reads as

$$H(\rho, \psi, \beta, v, \omega) = 1 - \lambda_1 \cos\beta v + \lambda_2 \frac{\sin\beta}{\rho}v + \lambda_3\left(\frac{\sin\beta}{\rho}v - \omega\right),$$

and the minimum H_{min} over $\mathcal{U}$ is therefore achieved taking $-\lambda_3\omega \leq 0$ and

$$v = -\text{sign}\left(-\lambda_1\cos\beta + \lambda_2\frac{\sin\beta}{\rho} + \lambda_3\frac{\sin\beta}{\rho}\right)(1 - b|\omega|).$$

The optimal controls are thus determined by the switching functions $\xi_1 := b\left|-\lambda_1\cos\beta + \lambda_2\frac{\sin\beta}{\rho} + \lambda_3\frac{\sin\beta}{\rho}\right|$ and $\xi_2 = |\lambda_3|$, i.e.

$$H_{min} = 1 - \xi_1 + |\omega^*|(\xi_1 - \xi_2),$$

with

$$|\omega^*| = \begin{cases} 0 & \text{if } \xi_1 \geq \xi_2 \\ \frac{1}{b} & \text{if } \xi_1 < \xi_2. \end{cases}$$

Consistently with the optimal solutions proposed in [12], the unconstrained extremals are rotations on the spot (denoted by $*$) covered at maximum angular

velocity and the straight lines (denoted by S) covered at maximum speed. For reader convenience, we explicitly report controls v and ω along such extremals

$$\begin{cases} v = 0 \\ \omega = \pm\frac{1}{b} \end{cases} \quad \text{or} \quad \begin{cases} v = \pm 1 \\ \omega = 0. \end{cases}$$

3.2 Constrained Arcs

Let us assume now that in the interval $[t_1, t_2]$ with $t_2 > t_1$ one of the FOV constraints is active, i.e. one of the conditions (5) and (6) is verified with the equality sign. For the H-FOV, given $q = (\rho, \psi, \beta)$ with $(\rho,\, \psi) \in Z_2$, we have $\beta \equiv \phi_i$ and hence $\tan\beta = \tan\phi_i$ with $i = 1$ or $i = 2$. Given the kinematic model (2), $\dot{\psi} = -\tan\phi_i \frac{\dot{\rho}}{\rho} = -\tan\phi_i \frac{d}{dt}(\ln\rho)$. By integration, we obtain the equation of a logarithmic spiral (see [17] for details)

$$\psi = -\tan\phi_i \ln\left(\frac{\rho}{\rho_0}\right) + \psi_0, \quad \text{or} \quad \rho = \rho_0 e^{-(\psi-\psi_0)\cot\phi_i}, \tag{11}$$

where $(\rho_0,\, \psi_0)$ is a point on the logarithmic spiral.

On the orther hand, the V-FOV constraint is activated for those configurations $q = (\rho, \psi, \beta)$ with $(\rho,\, \psi) \in Z_1$ and

$$\rho\cos(\beta - \Gamma) = R_b. \tag{12}$$

Given the kinematic model (2), the relationship between the control inputs v and ω required to follow a path along which (12) holds is given by

$$\dot{\rho}\cos(\beta-\Gamma) - \rho\sin(\beta-\Gamma)\dot{\beta} = 0 \Rightarrow \rho\sin(\beta-\Gamma)\omega = v\cos\Gamma.$$

From (2), the trajectory followed with such inputs satisfies

$$\dot{\psi} = -\tan\beta\tan(\beta-\Gamma)\ \dot{\beta}$$

that by integration gives the following relation between ψ and β,

$$\psi = \psi_b + \beta - \Gamma - \frac{\log\left(\cos^2\Gamma\left(1+\tan\beta\tan\Gamma\right)\right)}{\tan\Gamma}, \tag{13}$$

where ψ_b depends on the initial conditions. It is worth noting that the above expression is finite, and hence well-defined, also for $\Gamma \to 0$ and for $\Gamma \to \pi/2$. In particular, for $\Gamma = 0$ the equation corresponds to an *involute of a circle*[1] with polar coordinates expressed by:

$$\begin{cases} \rho\cos\beta = R_b \\ \\ \psi = \psi_b - \tan\beta + \beta\,. \end{cases} \tag{14}$$

For the involute of circle, when on C_b (i.e. $\rho = R_b$) the vehicle may only be directed toward the landmark in the origin, i.e. $\beta = 0$. On the other hand, for the general case $\Gamma \neq 0$ while on C_b the vehicle has $\beta = \Gamma$. Even if (12) and (13) do not correspond to an involute of circle, with an abuse of notation, in the following, we will still refer to this curve as an involute of circle.

Concluding, in Z_2 extremal arcs are logarithmic spirals with characteristic angle ϕ_1 and ϕ_2, respectively, rotating around the landmark located in O_w. Logarithmic spirals with characteristic angle $\phi_i < 0$ rotate clockwise around O_w (referred to as *Left* and denoted by symbol T_i^L), whereas with $\phi_i > 0$ they rotate counterclockwise around O_w (referred to as *Right* and denoted by symbol T_i^R). Note that, for $\phi_2 = \pi/2$ the left sensor border is perpendicular to the forward direction and by equation (11) (with $i = 2$) we have $\rho = \rho_0$,

[1] The involute of a circle is the path traced out by a point on a straight line r that rolls around a circle without slipping.

and hence, the extremal arc is a circle centered in O_w and radius ρ_0 (denoted by C_{O_w}). For $\phi_1 = 0$ the right sensor border is aligned with the direction of motion, and hence when the corresponding constraint is active we have $\beta = 0$. In this case, the extremal arc is an half–line through O_w (denoted by S_{O_w}). In other words, when $\phi_2 = \pi/2$ spiral T_2^R degenerates in a circle centered in O_w, whereas when $\phi_1 = 0$ spirals T_1^R and T_1^L degenerate in the same half–line through O_w.

In Z_1 extremal arcs are involutes of circle evolving clockwise and counterclockwise. Hence, similarly to the logarithmic spiral, we denote such extremals by I^R and I^L, respectively. Notice that, in case of $\Gamma = \pi/2$, (12) becomes $\rho \sin\beta = R_b$. To maintain the vehicle on a path along which previous equality holds, its first derivative has to be zero, i.e. $\omega\rho\cos\beta = 0$. This holds either if $\omega = 0$, that is the vehicle moves along a straight line tangent to the circumference C_b (denoted by S_b), or $\beta = \pi/2$, that is the vehicle moves along a circumference with radius $\rho = R_b$, i.e. circumference C_b.

It is worth noting that all extremal arcs can be executed by the vehicle in either forward ($v > 0$) or backward ($v < 0$) direction: we will hence use superscripts $+$ and $-$ to make this explicit (e.g. T^{R-} stands for a right spiral line executed backward).

To conclude, the optimal trajectories are concatenations of extremal paths $E \in \mathcal{E}$, with

$$\mathcal{E} = \{*, S, T_1^+, T_1^-, T_2^+, T_2^-, I^{R+}, I^{R-}, I^{L+}, I^{L-}\}\,, \tag{15}$$

where the value and the sign of ϕ_i determine if $T_i^{\pm}$ is a left spiral, a right spiral, C_{O_w} or S_{O_w}, and for this reason the symbols R, L in the expression of spirals in (15) have been omitted to keep the framework as much general as possible.

From a robotic point of view, it is also important to characterize the optimal controls w_R and w_L which are the real inputs of the dynamic system. The Hamiltonian function (10) in terms of inputs w_L and w_R, is

$$H = 1 + \frac{w_R}{2} s_+ + \frac{w_L}{2} s_- + \frac{w_R}{2} m_+ + \frac{w_L}{2} m_-,$$

where

$$\begin{aligned}
s_+ &= -\lambda_1 \cos\beta + \lambda_2 \tfrac{\sin\beta}{\rho} + \lambda_3 \tfrac{\sin\beta}{\rho} - \tfrac{\lambda_3}{b}, s_- = s_+ + 2\tfrac{\lambda_3}{b}, \\
m_+ &= (\mu_1 - \mu_2)\left(\tfrac{-\sin\beta}{\rho} + \tfrac{1}{b}\right) + \mu_3\left(\cos\Gamma - \tfrac{\rho\sin(\beta-\Gamma)}{b}\right), \\
m_- &= m_+ - 2(\mu_1 - \mu_2)\tfrac{1}{b} + 2\mu_3 \tfrac{\rho\sin(\beta-\Gamma)}{b},
\end{aligned}$$

with $\mu_1, \mu_2, \mu_3 \geq 0$. From Remark 2.1, one has necessarily $\mu_1\mu_2 = 0$ and $(\mu_1 + \mu_2)\mu_3 = 0$, that is the three constraints cannot be active simultaneously pairwise except than on C_S. Hence we can focus on the derivatives of the constraints activated in $[t_1, t_2]$, as function of w_R, w_L, for the H-FOV and the V-FOV cases separately.

3.2.1 Optimal Controls Along Spiral Arcs

In case of equality verification of the H–FOV constraints we have

$$\dot{\beta} = \frac{\sin\beta(w_R + w_L)}{2\rho} - \frac{w_R - w_L}{2b} = 0. \tag{16}$$

Hence for $\beta = \phi_i$ $i = 1, 2$, from (16), the two wheels velocities must satisfy

$$w_R \left(\rho - b \sin \phi_i\right) = w_L \left(\rho + b \sin \phi_i\right). \tag{17}$$

Since the H–FOV constraint is active the V–FOV one is verified as a strict inequalities in zone Z_2, i.e. $\mu_3 = 0$, and hence, from (17), the Hamiltonian can be rewritten in terms of w_R as

$$H = 1 + w_R r_+, \text{ where } r_+ = \left(\lambda_2 \sin \phi_i - \lambda_1 \rho \cos \phi_i\right) \frac{1}{\rho + b \sin \phi_i} \tag{18}$$

or equivalently in terms of w_L

$$H = 1 + w_L r_-, \text{ where } r_- = \left(\lambda_2 \sin \phi_i - \lambda_1 \rho \cos \phi_i\right) \frac{1}{\rho - b \sin \phi_i} \tag{19}$$

The Hamiltonian in (18) is minimized selecting $w_R = -\text{sign } r_+$. In this case $|w_R| = 1$ and from (17) $|w_L| \leq 1$ only if $\sin \phi_i \geq 0$. On the other hand, the Hamiltonian in (19) is minimized selecting $w_L = -\text{sign } r_-$. In this case $|w_L| = 1$ and from (17) $|w_R| \leq 1$ only if $\sin \phi_i < 0$.

Concluding, the spiral arc, represented by (16), is followed by the vehicle with the outer wheel having maximum velocity while the inner wheel velocity is given by (17). In other words, the controls that ensure the optimality of the spiral arc $T_i^{L\pm}$ are $w_L = \pm 1$ and $w_R = \pm \frac{\rho + b A_{T_i}}{\rho - b A_{T_i}}$ with $A_{T_i} = \sin \phi_i < 0$. For the spiral arc $T_i^{R\pm}$ the optimal controls are $w_R = \pm 1$ and $w_L = \pm \frac{\rho - b A_{T_i}}{\rho + b A_{T_i}}$ with $A_{T_i} = \sin \phi_i > 0$.

3.2.2 Optimal Controls Along Involute Arcs

Consider now the case in which the V–FOV constraint is activated. From (13), we have

$$\begin{aligned} &\frac{d}{dt}\left[\psi - \psi_b - \beta + \Gamma + \frac{\log\left(\cos^2\Gamma\,(1+\tan\beta\tan\Gamma)\right)}{\tan\Gamma}\right] \\ &= \dot{\psi} - \dot{\beta} + \frac{\cos\Gamma}{\cos\beta\cos(\beta-\Gamma)}\dot{\beta} = 0. \end{aligned} \tag{20}$$

From (2) and (20), the wheels velocities must satisfy the following relation:

$$w_R\left(\rho\sin(\beta-\Gamma) - b\cos\Gamma\right) = w_L\left(\rho\sin(\beta-\Gamma) + b\cos\Gamma\right). \tag{21}$$

From Remark 2.1 and the successive discussion, the H–FOV constraint is verified as a strict inequality in the interior part of Z_1 and hence $\mu_1 = \mu_2 = 0$. Thus, from (21), the Hamiltonian can be rewritten in the two equivalent forms in terms of w_R and w_L respectively

$$H = 1 + w_R t_+ \tag{22}$$

$$H = 1 + w_L t_-, \tag{23}$$

where

$$\begin{aligned} t_+ &= \frac{\lambda_3\cos\beta\cos(\beta-\Gamma) + (\lambda_1\rho\cos\beta - \lambda_2\sin\beta)\sin(\beta-\Gamma)}{b\cos\Gamma + \rho\sin(\beta-\Gamma)} \\ t_- &= \frac{\lambda_3\cos\beta\cos(\beta-\Gamma) + (\lambda_1\rho\cos\beta - \lambda_2\sin\beta)\sin(\beta-\Gamma)}{b\cos\Gamma - \rho\sin(\beta-\Gamma)}. \end{aligned}$$

The Hamiltonian in (22) is minimized selecting $w_R = -\text{sign}\, t_+$. In this case $|w_R| = 1$ and from (21) $|w_L| \leq 1$ only if $\beta \in [0,\, \pi/2]$ and hence $\sin\beta \geq 0$. On the other hand, the Hamiltonian in (23) is minimized selecting $w_L = -\text{sign}\, t_-$.

Arc type	w_R	w_L
$S^{\pm}$	$\pm\frac{1}{2}$	$\pm\frac{1}{2}$
$*$	± 1	∓ 1
$I^{\pm}$	$\pm\min\left\{1, \frac{\rho+bA_I}{\rho-bA_I}\right\}$	$\pm\min\left\{1, \frac{\rho-bA_I}{\rho+bA_I}\right\}$
$T_i^{\pm}$	$\pm\min\left\{1, \frac{\rho+bA_{T_i}}{\rho-bA_{T_i}}\right\}$	$\pm\min\left\{1, \frac{\rho-bA_{T_i}}{\rho+bA_{T_i}}\right\}$

Table 1 Optimal controls w_R and w_L along extremals, $A_{T_i} = \sin\phi_i$ and $A_I = \frac{\cos\Gamma}{\sin(\beta-\Gamma)}$.

In this case $|w_L| = 1$ and from (21) $|w_R| \leq 1$ only if $\beta \in [-\pi/2, 0]$ and hence $\sin\beta < 0$.

Concluding, the involute is followed by the vehicle when the outer wheel has maximum angular velocity while the inner wheel velocity is given by (21). The controls that ensure the optimality of the involute arc $I^{L\pm}$ are $w_L = \pm 1$ and $w_R = \pm\frac{\rho+bA_I}{\rho-bA_I}$ where $A_I = \frac{\cos\Gamma}{\sin(\beta-\Gamma)}$. While, for the involute arc $I^{R\pm}$, we have $w_R = \pm 1$ and $w_L = \pm\frac{\rho-bA_I}{\rho+bA_I}$.

For the sake of clarity, in tables 1 and 2, the state feedback expressions of optimal controls along the extremal arcs in $\mathcal{E}$ are reported.

Remark 3.1. It is worth to note that the motion along the differentiable path I^-T^- or T^+I^+ requires non–smooth control inputs (v, ω). Let us denote by G the intersection point (on C_S) between two curves I and T when the robot reaches the position G, a jump discontinuity appears in the control laws (17)-

Arc type	v	ω
$S^{\pm}$	± 1	0
$*$	0	$\pm\frac{1}{b}$
$I^{\pm}$	$\pm\min\left\{\frac{\rho}{\rho+bA_I}, \frac{\rho}{\rho-bA_I}\right\}$	$\pm\min\left\{\frac{A_I}{\rho+bA_I}, \frac{A_I}{\rho-bA_I}\right\}$
$T_i^{\pm}$	$\pm\min\left\{\frac{\rho}{\rho+bA_{T_i}}, \frac{\rho}{\rho-bA_{T_i}}\right\}$	$\pm\min\left\{\frac{A_{T_i}}{\rho+bA_{T_i}}, \frac{A_{T_i}}{\rho-bA_{T_i}}\right\}$

Table 2 Optimal controls v and ω along extremals, $A_{T_i} = \sin\phi_i$ and $A_I = \frac{\cos\Gamma}{\sin(\beta-\Gamma)}$.

(21). Indeed, the curvature along extremals $T^{L\pm}$ and $I^{L\pm}$ is given by $\frac{\omega}{v} = \pm\frac{A}{\rho}$ with $A = A_{T_i}$ and A_I respectively. In $G \in C_S$ it holds $\rho_S = \frac{R_b}{\cos\phi}$ and $\beta = \phi = \Gamma - \phi_1 = \phi_2 - \Gamma$. Hence

$$\frac{\omega}{v} = \frac{\sin\phi_i\cos(\phi_i - \Gamma)}{R_b} \quad \text{in } G \text{ as point of } T_i$$
$$\frac{\omega}{v} = \frac{\cos\Gamma}{R_b\tan(\phi_i - \Gamma)} \quad \text{in } G \text{ as point of } I$$

4 Controllability and Existence of Optimal Trajectories

The necessary conditions, obtained from the PMP and described in previous section, allow us to restrict to the set of extremal paths $\mathcal{E}$ as basic components for the construction of optimal trajectories. The study of time-optimal paths will be carried out addressing the following two main points: controllability of the system and existence of optimal solutions. Regarding controllability it holds the following

Proposition 4.1 *Given two arbitrary positions Q and P outside Z_0, there always exists a trajectory from Q to P for the system* (2) *with constraints* (5) *and* (6).

Proof. Consider the families of extremal paths of type $T_1^{\pm}, T_2^{\pm}, I^{R\pm}, I^{L\pm}$. Assume $Q, P \in Z_2$ first. Given the initial point Q, there exists a unique T_1 curve containing such point, say $T_{1,Q}$; on the other hand, there exists a unique T_2 curve, say $T_{2,P}$, passing through the final position P. The curves $T_{1,Q}$ and $T_{2,P}$ do always have intersection points: let us select and denote by Y one of such points. Moving from Q along the curve $T_{1,Q}$ until reaching Y, rotating towards the origin, and hence towards the feature, and then moving along $T_{2,P}$ until the final position P, the vehicle can reach the target point without violating the H–FOV constraints. The same it's true if one changes the roles of T_1 and T_2.

Now, by construction, the radius ρ always evolves monotonically along the curves T_1, T_2; moreover, one can adopt one of the proposed schemes $T_{1,Q} \circ T_{2,P}$ or $T_{2,Q} \circ T_{1,P}$ in such a way that the radius is increasing along the first curve. Consequently, whenever $Q, P \in Z_2$, a feasible trajectory exists.

On the other hand if P lies inside the region Z_1, this can be connected to a point Q' on C_S by a curve of type I^R (or I^L): thus, using the previous argument, a feasible trajectory is given by one of the combinations $I_Q^R \circ T_{1,Q'} \circ T_{2,P}$, $I_Q^R \circ T_{2,Q'} \circ T_{1,P}$. By symmetry, a similar strategy can be defined in the case $Q \in Z_2$ and $P \in Z_1$: denoting by P' the intersection point between C_S and the involute curve of type I^L (or I^R) from P, a feasible path is then given by

$T_{1,Q} \circ T_{2,P'} \circ I_P^L$ or $T_{2,Q} \circ T_{1,P'} \circ I_P^L$.

In the last case with both $Q, P \in Z_1$, a feasible path is obtained by combining the previous schemes, this leading to a general abstract structure for admissible trajectories: $I \circ T \circ T \circ I$. Taking into account initial and final orientations also, rotations on the spot $*$ can be used for aligning the heading to, respectively, the first and the last curve of the combination: $* \circ I \circ T \circ T \circ I \circ *$. □

The existence of time-optimal trajectories will now be proved.

Theorem 4.1 *For any given positions $P, Q \notin Z_0$ there exists a solution $(v_{opt}, \omega_{opt}) \in \mathcal{U}$ to the optimal control problem 2.1.*

Proof. Due to controllability, convexity of the control space $\mathcal{U}$ and closedness of the state constraint set $\mathcal{S}$, the existence of optimal controls can be deduced from the well known Filippov Theorem [38–40]. □

5 Time Costs Along Extremal Arcs

Given a path γ from Q_1 to Q_2, we denote by $\mathcal{T}^\star(\gamma, \beta_{Q_1}, \beta_{Q_2})$ the time cost associated to γ with prescribed initial and final orientations β_{Q_1}, β_{Q_2}. We, thus, denote by $\mathcal{T}_\gamma = \min_{\beta_{Q_1}, \beta_{Q_2}} \mathcal{T}^\star(\gamma, \beta_{Q_1}, \beta_{Q_2})$.

We are now interested in computing the time costs $\mathcal{T}_E$ associated to extremal arcs $E \in \mathcal{E}$ defined in (15). Recalling that $|v| \leq 1$ and $b|\omega| \leq 1 - |v|$, the case of unconstrained arcs is trivial but reported for completeness.

Proposition 5.1 *The time cost $\mathcal{T}_S(Q_1, Q_2)$ of a straight arc S from Q_1 to Q_2, is equal to the distance between the two points:*

$$\mathcal{T}_S(Q_1, Q_2) = dist(Q_1, Q_2) = \overline{Q_1 Q_2}. \tag{24}$$

Proposition 5.2 *The time cost $\mathcal{T}_*(\beta)$ of a rotation on the spot of an angle β, is given by*

$$\mathcal{T}_*(\beta) = b|\beta|.$$

The proofs of the following propositions on involutes and spirals costs can be found in [27]. The statements are reported for reader convenience.

Proposition 5.3 *Given an arc of logarithmic spiral T_i, with characteristic angle ϕ_i, from $Q_1 = (\rho_{Q_1}, \psi_{Q_1})$ to $Q_2 = (\rho_{Q_2}, \psi_{Q_2})$, the time cost $\mathcal{T}_T(Q_1, Q_2)$ is*

$$\mathcal{T}_T(Q_1, Q_2) = \frac{|\rho_{Q_1} - \rho_{Q_2}|}{\cos\phi_i} + b|\psi_{Q_1} - \psi_{Q_2}|.$$

The time $\mathcal{T}_T(Q_1, Q_2)$ is hence given by the sum of the length of the spiral between Q_1 and Q_2 and the time equivalent to a rotation on the spot of an angle $|\psi_{Q_1} - \psi_{Q_2}|$.

Remark 5.1. As mentioned in Section 3.2, for $\phi_2 = \pi/2$ the extremal arc becomes a circle, denoted by C, centered in O_w and radius ρ_o. The time-cost from $Q_1 = (\rho_o, \psi_{Q_1})$ to $Q_2 = (\rho_o, \psi_{Q_2})$ on C is $\mathcal{T}_C = (\rho_o + b)|\psi_{Q_1} - \psi_{Q_2}|$. On the other hand, for $\phi_1 = 0$ the extremal arc becomes a straight line, denoted by H, through O_w. The time-cost $\mathcal{T}_H$ from Q_1 to Q_2 on H is given by (24).

Proposition 5.4 *Given an arc of involute I from* $Q_1 = (\rho_{Q_1}, \psi_{Q_1})$ *to* $Q_2 = (\rho_{Q_2}, \psi_{Q_2})$*, the time cost* $\mathcal{T}_I(Q_1, Q_2)$ *is*

$$\mathcal{T}_I(Q_1, Q_2) = R_b(\zeta_v(\beta_{Q_2}, \Gamma) - \zeta_v(\beta_{Q_1}, \Gamma)) + b(\zeta_\omega(\beta_{Q_2}, \Gamma) - \zeta_\omega(\beta_{Q_1}, \Gamma)),$$

where $\beta_{Q_i} = \arccos(R_b/\rho_{Q_i}) + \Gamma$, $i = 1, 2$ *and*

$$\zeta_v(\beta, \Gamma) = \left(\frac{\cot\Gamma}{\sin\Gamma}\log\left(\frac{\cos(\beta-\Gamma)}{\cos\beta}\right) - \frac{2\sin\beta}{\sin 2\Gamma\cos(\beta-\Gamma)}\right)$$

$$\zeta_\omega(\beta, \Gamma) = \cot\Gamma\left(\log\left(\tfrac{\cos(\beta-\Gamma)}{\cos\beta}\right)\right).$$

Remark 5.2. In the symmetric case $\Gamma = 0$ the expression of the time cost $\mathcal{T}_I(Q_1, Q_2)$ is

$$\mathcal{T}_I(Q_1, Q_2) = \frac{R_b}{2}(\tan^2\beta_{Q_2} - \tan^2\beta_{Q_1}) + b(\tan\beta_{Q_2} - \tan\beta_{Q_1}). \tag{25}$$

The time $\mathcal{T}_I(Q_1, Q_2)$ is hence given by the sum of the length of the involute between Q_1 and Q_2 and the time equivalent to a rotation on the spot of an angle $|\tan\beta_{Q_1} - \tan\beta_{Q_2}|$.

Remark 5.3. As shown in Section 3.2, for $\Gamma = \pi/2$, involutes of circle degenerate in straight line H_b tangent to the circumference C_b and the circumference C_b itself. In the first case the time-cost $\mathcal{T}_{H_b}$ from Q_1 to Q_2 on H_b is given by (24), while in the second case the time-cost from Q_1 to Q_2 on C_b is $\mathcal{T}_{C_b} = R_b b|\tan\beta_{Q_1} - \tan\beta_{Q_2}|$.

6 Analysis of the Junction Times Set

In Section 3 it has been shown that optimal trajectories can be regarded as combinations of extremal arcs $E \in \mathcal{E}$; with the aim of giving a characterization

of such concatenations, the following question arise.

Question. May time-optimal trajectories obtained as combinations of infinitely many extremal arcs exist for some particular choices of initial/final configurations?

The question arises since optimal paths with an infinite number of extremals exist in the minimum length control problem described in [18] and [20]. In this section we will focus on addressing formally this problem for the minimum time case. In particular, it will be proved that time optimal trajectories cannot have infinitely many switching points between different extremal arcs. Hence infinite sequences of symbols T, I or S are never included in the "language" describing optimal paths that is hence finite. To this end, the following definition will be helpful [33].

Definition 6.1 Let be $s(x(t)) \leq 0$ an arbitrary unilateral state-space constraint for the system.

- If $s(x(t)) < 0$ for any $t \in]t_1 - \delta, t_1[\bigcup]t_1, t_1 + \delta[$ for some $\delta > 0$, while $s(x(t_1)) = 0$, then t_1 is called **touch time**.
- If $s(x(t)) < 0$ for any $t \in]t_2 - \epsilon, t_2[\bigcup]t_3, t_3 + \eta[$ for some $\epsilon, \eta > 0$ and $s(x(t)) = 0$ for any $t \in [t_2, t_3]$, then t_2 is called **entry time** and t_3 is called **exit time**.

– The family constituted by touch times and entry/exit times is called the set of **junction times**.
– The set of all times t such that $s(x(t)) = 0$ is called **contact times** set.

According to the previous definition, we will call touch/junction/contact points the vehicle configurations corresponding to touch/junction/contact times.

The main contribution of this paper is the proof that in any optimal trajectory the set of junction times is finite. In other words:

Theorem 6.1 *Optimal trajectories are composed of a finite number of extremal concatenations.*

The proof of this theorem will follow from the results described next. For the sake of simplicity we will consider the symmetric case only, i.e. $\Gamma = 0$. However, the case $\Gamma \neq 0$ can be analyzed with the same approach.

As a first result we have that infinite switches may occur only on the circumference C_b. Indeed, it holds

Proposition 6.1 *Any optimal path with an infinite junction time set has only a finite number of junction points outside C_b.*

Proof. The time cost of involutes and spirals is given by sum of the length of the arc and an angular contribution: using this fact, together with some elementary geometry, it can be inherited from the synthesis results obtained in [17, 20, 32] for minimal length paths that the only types of arcs that are allowed to be repeated several times in a feasible time-optimal path away from the circle C_b are spirals and involutes. In particular, following the arguments

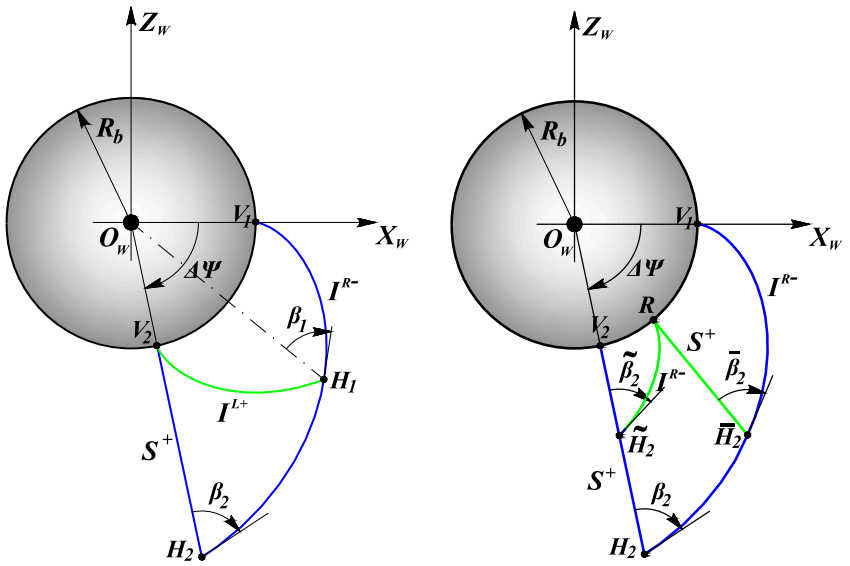

(a) Construction of paths $\gamma_I(\Delta\psi) = I^{R-} * I^{L+}$ and $\gamma_S(\Delta\psi) = I^{R-} * S^+$ from V_1 to V_2 on C_b.

(b) Construction of paths $\gamma_S(\bar{\beta}_2) = I^{R-} * S^+$ from V_1 to R and $\gamma_S(\tilde{\beta}_2) = I^{R-} * S^+$ from R to V_2.

Fig. 3 Graphical construction for the proof of: (a) Proposition 6.2, (b) Proposition 6.3.

of [17, Proposition 10] and [20, Proposition 3] and observing that the time cost of a straight line equals its length, the concatenation of more than two extremals of type $S^{\pm}$ is proved to be never optimal. On the other hand, from Proposition 5.2, the junction points between spirals T_i, T_j are associated to a fixed angular time cost $\mathcal{T}(*_{|\phi_i - \phi_j|}) = b|\phi_i - \phi_j| > 0$ and hence, for any feasible trajectory, these can be at most finitely many. A similar condition holds true for the case of switching between involutes I_R, I_L in a point $Q = (\rho_Q, \psi_Q)$ with $\beta_Q > 0$. Hence, it has been proved that infinite junction points may occur only for $\beta_Q = 0$, i.e. on the circumference C_b. □

As a consequence, we can restrict the analysis to the case of vertical constraints, focusing on touch points placed on the circle C_b, i.e. where $\beta = 0$.

Hence, we now consider the possible extremals concatenations between any two points on C_b and we analyze the time cost of such paths. For this purpose, and without loss of generality, consider two touch points $V_1 = (R_b, 0)$ and $V_2 = (R_b, \Delta\psi)$ on C_b, with $\Delta\psi < 0$, see Fig. 3(a). Consider now two paths from V_1 to V_2 composed by two extremals. The first is $\gamma_I(\Delta\psi) = I^{R-} * I^{L+}$, i.e. a pair of symmetric involute arcs with intersection point $H_1 = (\rho_1, \psi_1)$. At the end of extremal I^{R-}, i.e. in H_1, the vehicle bearing angle is $\beta_1 > 0$. The second paths is $\gamma_S(\Delta\psi) = I^{R-} * S^+$, i.e. an involute arc and a straight line intersecting in $H_2 = (\rho_2, \psi_2)$. At the end of extremal I^{R-}, i.e. in H_2, the vehicle bearing angle is $\beta_2 > 0$. It is worth noting that, since $V_2 \in C_b$, it holds $\beta_{V_2} = 0$ and hence the point V_2 can be reached with a straight line, without violating the vertical constraints, only if the line is directed toward the origin. As a consequence it holds $\psi_2 = \Delta\psi = 2\psi_1$ and hence, since H_1 and H_2 lays on the same involute, the bearing angle β_1 and β_2 must satisfy: $\beta_1 < \beta_2$ and (from the second equation of the involute (14))

$$2(\beta_1 - \tan\beta_1) = \beta_2 - \tan\beta_2. \tag{26}$$

With an abuse of notation we consider the paths γ_I and γ_S as dependent on variables β_1 and β_2 respectively. Indeed β_1 and β_2 can be obtained solving equations $\beta_1 - \tan\beta_1 = \frac{\Delta\psi}{2}$ and $\beta_2 - \tan\beta_2 = \Delta\psi$.

For symmetry in the path, the time cost for travelling along $\gamma_I(\beta_1)$ doubles the time of path I from V_1 to H_1. Hence, from (25), considering $Q_1 = V_1 \in C_b$

and $Q_2 = H_1$ we have $\beta_{Q_2} = \beta_1$ and $\beta_{Q_1} = 0$ and hence the time cost for travelling along $\gamma_I(\beta_1)$ is

$$\mathcal{T}(\gamma_I(\beta_1)) = R_b \tan^2 \beta_1 + 2b \tan \beta_1 + 2b\beta_1, \tag{27}$$

On the other hand, the time cost of path $\gamma_S(\beta_2)$ is given by the sum of the time costs of I from V_1 to H_2 and S from H_2 to V_2. Hence, from (25), considering $Q_1 = V_1 \in C_b$ and $Q_2 = H_2$ we have $\beta_{Q_2} = \beta_2$, $\beta_{Q_1} = 0$. The time cost for travelling along $\gamma_S(\beta_2)$ is

$$\mathcal{T}(\gamma_S(\beta_2)) = \frac{R_b}{2} \tan^2 \beta_2 + b \tan \beta_2 + b\beta_2 + R_b \left(\frac{1}{\cos \beta_2} - 1 \right), \tag{28}$$

where the linear terms $2b\beta_1$ and $b\beta_2$, in (27) and (28), are the time cost of rotations on the spot in the points H_1 and H_2, respectively. In the rest of the Section we will prove that, for sufficiently small values of angle β_i, the path $\gamma_S(\beta_2)$ is the one covered with smallest time with respect to all other possible paths from V_1 to V_2. We start proving that for small values of angles β_1 and β_2, a curve of type γ_S is more convenient than a curve γ_I. In other words

Proposition 6.2 *There exists $\zeta_0 > 0$ such that*

$$\mathcal{T}(\gamma_S(\beta_2)) < \mathcal{T}(\gamma_I(\beta_1)) \qquad \forall \beta_1 < \beta_2 < \zeta_0 \tag{29}$$

Proof. In order to compare time costs (27) and (28), let us define the function

$$\Psi(x) := \tan(x) - x. \tag{30}$$

For $0 \leq x \leq 1$, from the Taylor expansion of $\Psi(x)$, it holds

$$\frac{1}{3}x^3 \leq \Psi(x) \leq c_1 x^3, \tag{31}$$

where $c_1 = \tan(1) - 1$. From (26) and the inequalities (31) for β_1 and β_2, assuming $\beta_1 < \beta_2 < 1$, one can infer that

$$\sqrt[3]{\frac{2}{3c_1}}\beta_1 \leq \beta_2 \leq \sqrt[3]{6c_1}\beta_1,$$

with $\ell_0 := \sqrt[3]{6c_1} < 2$. From the first order Taylor expansion of time costs (27) and (28) we have $\mathcal{T}(\gamma_I(\beta_1)) \approx 4b\beta_1$ and $\mathcal{T}(\gamma_S(\beta_2)) \approx 2b\beta_2 \leq 2b\ell_0\beta_1 < 4b\beta_1$, hence the thesis with $\zeta_0 = 1$. □

We can now proceed considering more complex paths from V_1 to V_2. In order to study the existence of path with infinite junction times we continue to consider paths with junction points on C_b. All such paths from V_1 to V_2 consist in concatenations of paths of type $I^{R-} * I^{L+}$ and $I^{R-} * S^{+}$. We will prove that $\gamma_S(\beta_2)$ has time cost less than any of those paths for sufficiently small values of β_2.

From Proposition 6.2 for sufficiently small angles β we only need to compare the time cost of a single path $I^{L-} * S^{+}$ with the ones of multiple sequences of paths of the same type. For this purpose, referring to Fig. 3(b), let us now consider a point $R \in C_b$ between V_1 and V_2 and two paths $\gamma_S(\bar{\beta}_2) = I^{R-} * S^{+}$ from V_1 to R and $\gamma_S(\tilde{\beta}_2) = I^{R-} * S^{+}$ from R to V_2 such that $\bar{\beta}_2, \tilde{\beta}_2 < \beta_2$ and

$$\bar{\beta}_2 - \tan\bar{\beta}_2 + \tilde{\beta}_2 - \tan\tilde{\beta}_2 = -\Psi(\bar{\beta}_2) - \Psi(\tilde{\beta}_2) = -\Psi(\beta_2) = \Delta\Psi. \tag{32}$$

The physical meaning of (32) is that the concatenation of $\gamma_S(\bar{\beta}_2)$ with $\gamma_S(\tilde{\beta}_2)$ provides a path from V_1 to V_2 as $\gamma_S(\beta_2)$ does. The equation is written in terms of the variation of angles ψ along the paths.

In order to compare $\mathcal{T}(\gamma_S(\beta_2))$ with $\mathcal{T}(\gamma_S(\bar{\beta}_2)) + \mathcal{T}(\gamma_S(\tilde{\beta}_2))$ we will use the following inequality proved in Appendix 8.1.

Lemma 6.1 *Let $\Psi(x)$ be the function defined in* (30)*; then, for any $x, y > 0$ one has*

$$\Psi^{-1}(\Psi(x) + \Psi(y)) < \sqrt[3]{x^3 + y^3}.$$

Proposition 6.3 *There exists $\zeta_1 > 0$ such that, if $\beta_2 < \zeta_1$,one has*

$$\mathcal{T}(\gamma_S(\beta_2)) < \mathcal{T}(\gamma_S(\bar{\beta}_2)) + \mathcal{T}(\gamma_S(\tilde{\beta}_2)). \tag{33}$$

for any $\bar{\beta}_2$, $\tilde{\beta}_2 < \beta$ verifying (32)*.*

Proof. From (28), the time-cost associated to a curve $\gamma_S(\beta)$ between points on C_b is:

$$f(\beta) := \mathcal{T}(\gamma_S(\beta)) = \frac{R_b}{2}\left(\frac{1}{\cos^2\beta} - 1\right) + R_b\left(\frac{1}{\cos\beta} - 1\right) + b\tan\beta + b\beta.$$

From (32) we have $\beta_2 = \Psi^{-1}(\Psi(\bar{\beta}_2) + \Psi(\tilde{\beta}_2))$, and since $f(\cdot)$ is an increasing function, by Lemma 6.1 it follows

$$f(\beta_2) < f\left(\sqrt[3]{\bar{\beta}_2^3 + \tilde{\beta}_2^3}\right).$$

In order to prove the thesis we now need to prove the following inequality

$$f\left(\sqrt[3]{\bar{\beta}_2^3 + \tilde{\beta}_2^3}\right) < f(\bar{\beta}_2) + f(\tilde{\beta}_2).$$

This will be proved for each addendum in $f(\cdot)$. For the linear addendum $b\beta$, from the properties of subadditivity of concave functions we have $b\sqrt[3]{\beta_2^3 + \tilde{\beta}_2^3} <$

$b(\beta_2 + \tilde{\beta}_2)$.

The inequality for term $b \tan \beta_2$ is equivalent to the positiveness of function

$$h_0(x) = \tan x + \tan y - \tan \sqrt[3]{x^3 + y^3},$$

for fixed $y > 0$. We have $h_0(0) = 0$ and

$$h_0'(x) = x^2 \left(\frac{1}{x^2 \cos^2 x} - \frac{1}{(x^3 + y^3)^{\frac{2}{3}} \cos^2 \sqrt[3]{x^3 + y^3}} \right) > 0, \text{ for } \sqrt[3]{x^3 + y^3} < \sqrt{2/3}.$$

Indeed function $p_0(s) = s \cos s$ is strictly increasing for $s \in \left[0, \sqrt{2/3}\right[$ since $p_0'(s) = \cos s - s \sin s > 1 - \frac{3}{2} s^2$.

The other terms in $f(\beta_2)$ depending on $\frac{1}{\cos \beta}$ and $\frac{1}{\cos^2 \beta}$ will be treated in a similar way. For fixed $y > 0$ we set

$$h_i(x) = \frac{1}{\cos^i x} + \frac{1}{\cos^i y} - \frac{1}{\cos^i \sqrt[3]{x^3 + y^3}}, \quad i = 1, 2.$$

We have that $h_i(0) = 0$ and

$$h_i'(x) = i x^2 \left(\frac{\sin x}{x^2 \cos^{i+1} x} - \frac{\sin \sqrt[3]{x^3 + y^3}}{(x^3 + y^3)^{\frac{2}{3}} \cos^{i+1} \sqrt[3]{x^3 + y^3}} \right).$$

Consider now the functions $p_i(s) = \frac{\sin s}{s^2 \cos^{i+1} s}$, $i = 1, 2$ that are the strictly decreasing for small $s > 0$. Indeed,

$$p_i'(s) = \frac{s \cos^2 s - 2 \cos s \sin s + (i+1) s \sin^2 s}{s^3 \cos^{i+2} s}$$

and $p_2'(s) < \frac{s(-1 + \frac{11}{3} s^2)}{s^3 \cos^3 s}$ while $p_3'(s) < \frac{s(-1 + \frac{14}{3} s^2)}{s^3 \cos^4 s}$.

Hence $p_2'(s) < 0$ for $s \in \left]0, \sqrt{3/11}\right[$ and $p_3'(s) < 0$ for $s \in \left]0, \sqrt{3/14}\right[$.

Since p_i are strictly decreasing, the functions $h_i(x)$ are positive and hence the inequality holds for both terms $\frac{1}{\cos^i \beta}$.

Summarizing, it has been shown that

$$f(\beta_2) < f(\bar{\beta}_2) + f(\tilde{\beta}_2)$$

for any $\bar{\beta}_2, \tilde{\beta}_2 \neq 0$ with $\sqrt[3]{\bar{\beta}_2^3 + \tilde{\beta}_2^3} < \sqrt{3/14}$; the statement of the proposition then follows with $\zeta_1 = \frac{1}{2}\sqrt{\frac{3}{14}}$ and hence the thesis. □

Remark 6.1. A straightforward consequence of Propositions 6.2 and 6.3 is that the trajectory γ_S has time cost strictly smaller than any concatenation of trajectories of type γ_I for sufficiently small angles.

We can finally prove Theorem 6.1. The proof is based on the idea that for any optimal trajectory with infinite junction points there always exist another trajectory with the same time cost in which there are three consecutive junction points that are sufficiently close to each other so that hypothesis of Proposition 6.3 are verified. Hence, a smaller time trajectory is found violating the assumption of optimality of the trajectory with infinite junction points.

of Theorem 6.1. Thanks to Proposition 6.1, we can restrict our focus on touch point lying on the circumference C_b. Let us denote by $J \subset C_b$ the set of touch points of the trajectory $q(t)$ on the set C_b, and by $\mathcal{Z} \subset [0, \infty[$ the corresponding set of times, i.e.

$$q(t) = [R_b \ \psi(t) \ 0] \in C_b \Rightarrow t \in \mathcal{Z}.$$

Now, if $q^*(t)$ is an optimal trajectory, the set $\mathcal{Z}$ does not contain any interval. In fact, suppose that t_1, t_2 exist with $q^*(t) \in C_b \ \forall t \in [t_1, t_2]$; then, since any absolute continuous function being constant on a non-degenerate interval has zero derivative a.e. in such interval, one has necessarily $\dot{\rho}^*(t) = 0$ for a.e.

$t \in [t_1, t_2]$ and this implies $v = \omega = 0$ a.e. in $[t_1, t_2]$. As a consequence, the state $q^*(t)$ is forced to be constant over the whole interval $[t_1, t_2]$ and this obviously contradicts the optimality of the trajectory. Let us prove now that the set J, or equivalently the set $\mathcal{Z}$, must have finite cardinality. By contradiction, assume that $t', t'' \in \mathcal{Z}$ with $t' < t''$ can be found such that the intersection $[t', t''] \cap \mathcal{Z}$ contains infinitely many times.

Now by construction, the set $\mathcal{Z}_0 := [t', t''] \cap \mathcal{Z}$ is closed and hence its complementary $\mathcal{Z}_1 = \mathbb{R} \setminus \mathcal{Z}_0$, which is open, can be represented as the union of a countable family of open intervals. Among such family, a subfamily of open intervals $\left\{]t_k^-, t_k^+[\right\}_{k \in \mathbb{N}}$ can be found such that

$$[t', t''] = \mathcal{Z}_0 \cup \bigcup_{k \in \mathbb{N}} \left] t_k^-, t_k^+ \right[.$$

Select any two intervals, say $\mathcal{I}_1 = \left] t_{k_1}^-, t_{k_1}^+ \right[$ and $\mathcal{I}_2 = \left] t_{k_2}^-, t_{k_2}^+ \right[$. Since the trajectories of the system admit left and right derivatives in the junction points, the portion of optimal trajectory $q^*(t)$ for $t \in \left] t_{k_1}^-, t_{k_2}^+ \right[$ can be decomposed as the union of curves of type γ_I or γ_S having extrema, respectively, in the pair of points $(q^*(t_{k_1}^-), q^*(t_{k_1}^+))$ and $(q^*(t_{k_2}^-), q^*(t_{k_2}^+))$ together with a path $\mathcal{X}$ connecting the point $q^*(t_{k_1}^+)$ to the point $q^*(t_{k_2}^-)$. The time cost is expressed as

$$\mathcal{T}(q^*(t))_{|_{t \in [t_{k_1}^-, t_{k_2}^+]}} = \mathcal{T}(\gamma_{\star_1}(\beta_{\star_1})) + \mathcal{T}(\chi) + \mathcal{T}(\gamma_{\star_2}(\beta_{\star_2})),$$

with

$$\beta_{\star_i} = \begin{cases} \Psi^{-1}\left(\frac{|\psi^*(t_{k_i}^+) - \psi^*(t_{k_i}^-)|}{2} \right) & \text{if } \star_i = I \\ \Psi^{-1}\left(|\psi^*(t_{k_i}^+) - \psi^*(t_{k_i}^-)| \right) & \text{if } \star_i = S \end{cases} \qquad i = 1, 2.$$

A time equivalent path $q^{**}(t)$ on $[t^-_{k_1}, t^+_{k_2}]$ with the same initial/final conditions can be constructed by switching the curves $\gamma_{\star_2}$ and χ, namely

$$q^{**}(t) := \begin{cases} q^*(t) & t \in [t^-_{k_1}, t^+_{k_1}] \\ q^*(t + t^-_{k_2} - t^+_{k_1}) & t \in \left]t^+_{k_1}, t^+_{k_1} + t^+_{k_2} - t^-_{k_2}\right] \\ q^*(t + t^-_{k_2} - t^+_{k_2}) & t \in \left]t^+_{k_1} + t^+_{k_2} - t^-_{k_2}, t^+_{k_2}\right] \end{cases}$$

where the chain of equalities $q^*(t^-_{k_1}) = q^*(t^+_{k_1}) = q^*(t^-_{k_2}) = q^*(t^+_{k_2}) = 0$ have been used. The time cost of $q^{**}(t)$ is then given by

$$\mathcal{T}(q^{**}(t))_{|_{t\in[t^-_{k_1}, t^+_{k_2}]}} = \mathcal{T}(\gamma_{\star_1}(\beta_{\star_1})) + \mathcal{T}(\gamma_{\star_2}(\beta_{\star_2})) + \mathcal{T}(\chi_\sharp),$$

where $\chi_\sharp$ is the shifted version of the path χ. Now, due to the assumption on the infinite number of touch points in J, the length of intervals $\left]t^-_{k_i}, t^+_{k_i}\right[$, $i = 1, 2$ can be chosen arbitrarily small and hence, without loss of generality, one can assume that $\beta_{\star_1}, \beta_{\star_2} < \min\{\zeta_0, \zeta_1, \zeta_2\}$. In force of Propositions 6.2 and 6.3, setting $\hat{\beta} = \Psi^{-1}(\Psi(\beta_{\star_1}) + \Psi(\beta_{\star_2}))$, one has

$$\mathcal{T}(\gamma_S(\hat{\beta})) < \mathcal{T}(\gamma_{\star_1}(\beta_{\star_1})) + \mathcal{T}(\gamma_{\star_2}(\beta_{\star_2})).$$

In this way, we have provided an extremal curve with a strictly minor time cost, this showing that the trajectory $q^{**}(t)$, and therefore also the very original one $q^*(t)$, cannot be optimal. In particular, it has been proved that the open set $\mathcal{Z}_1$ can always be decomposed as the union of a finite number of open intervals: as consequence the set $\mathcal{Z}_0$, which has been shown to contain no intervals, is necessarily formed by isolated elements, i.e. limit points are not admitted.

In conclusion, the touch points set J contains, at most, a finite number of points. □

7 Perspectives and Open Problems

Several issues remain to be further investigated. The final objective of the research study is a complete characterization of optimal trajectories for motion planning and visual–servoing purposes, as well as the development of control algorithms for efficiently steering the vehicle along the optimal path. In this regard, the following challenges are still open:

- Existence of an upper bound for the number of extremal arcs composing optimal trajectories.
- Decomposition of the state-space into regions corresponding to different concatenations of extremals, i.e. time optimal synthesis.
- Representation of optimal inputs as state-feedback controllers.
- Construction of numerical approximations of optimal paths and optimal control laws.

Since several other kinematic models are available besides the differential-drive one, it is certainly interesting, both from a theoretical and practical perspective, to investigate the extension of the optimality results to different types of non holonomic robots, such as car-like vehicles [24].

Moreover, it is also worth assessing the generalization of optimal path synthesis to higher order robotic systems, as suggested by the application-oriented papers [41, 42] where aerial and underwater robots with limited Field-of-View are considered.

8 Conclusions

In this paper the problem of time-optimal control of a non-holonomic vehicle subject to vision constraints has been considered. The existence of optimal trajectories has been proved for any possible choice of initial/final configurations; moreover, thanks to Pontryagin maximum principle, optimal paths can be represented as the concatenation of four possible types of extremal arcs: straight lines, rotations on the spot, logarithmic spirals and involutes of a circle. The main result of the paper is the proof that, for initial/final pose of the robot, the optimal trajectory has finitely many switching points between extremals.

References

1. Siegwart, R., Nourbakhsh, I.R., Scaramuzza, D.: Introduction to autonomous mobile robots. MIT press (2011)
2. Cortés, J., Martínez, S., Bullo, F.: Robust rendezvous for mobile autonomous agents via proximity graphs in arbitrary dimensions. Automatic Control, IEEE Transactions on **51**(8), 1289–1298 (2006)
3. Ghrist, R., Lavalle, S.M.: Nonpositive curvature and Pareto optimal coordination of robots. SIAM Journal on Control and Optimization **45**(5), 1697–1713 (2006)
4. Ghrist, R.W., Koditschek, D.E.: Safe cooperative robot dynamics on graphs. SIAM journal on control and optimization **40**(5), 1556–1575 (2002)
5. Guibas, L.J., Motwani, R., Raghavan, P.: The robot localization problem. SIAM Journal on Computing **26**(4), 1120–1138 (1997)
6. Zhou, X.S., Roumeliotis, S.I.: Robot-to-robot relative pose estimation from range measurements. Robotics, IEEE Transactions on **24**(6), 1379–1393 (2008)

7. Cristofaro, A., Martinelli, A.: Optimal trajectories for multi robot localization. In: Decision and Control (CDC), 2010 49th IEEE Conference on, pp. 6358–6364. IEEE (2010)

8. Dudek, G., Romanik, K., Whitesides, S.: Localizing a robot with minimum travel. SIAM Journal on Computing **27**(2), 583–604 (1998)

9. Ecker, J.G., Kupferschmid, M., Marin, S.P.: Performance of several optimization methods on robot trajectory planning problems. SIAM Journal on Scientific Computing **15**(6), 1401–1412 (1994)

10. Reeds, J.A., Shepp, L.A.: Optimal paths for a car that goes both forwards and backwards. Pacific Journal of Mathematics pp. 367–393 (1990)

11. Souères, P., Boissonnat, J.D.: Optimal Trajectories for Nonholonomic Mobile Robots, vol. 229. Lecture note in control and information scienze, H. Souères and J. P. Laumond (1998)

12. Balkcom, D., Mason, M.: Time optimal trajectories for bounded velocity differential drive vehicles. The International Journal of Robotics Research **21**(3), 199–217 (2002)

13. Hartley, R., Zisserman, A.: Multiple View Geometry in Computer Vision. Cambridge University Press (2003)

14. Gans, N., Hutchinson, S.: A stable vision-based control scheme for nonholonomic vehicles to keep a landmark in the field of view. In: Proc. IEEE Int. Conf. on Robotics and Automation, pp. 2196 –2201 (2007)

15. Gans, N., Hutchinson, S.: Stable visual servoing through hybrid switched system control. IEEE Transactions on Robotics **23**(3), 530–540 (2007)

16. Murrieri, P., Fontanelli, D., Bicchi, A.: A hybrid-control approach to the parking problem of a wheeled vehicle using limited view-angle visual feedback. Int. Jour. of Robotics Research **23**(4–5), 437–448 (2004)

17. Salaris, P., Fontanelli, D., Pallottino, L., Bicchi, A.: Shortest paths for a robot with nonholonomic and field-of-view constraints. IEEE Transactions on Robotics **26**(2), 269–281 (2010)

18. Salaris, P., Pallottino, L., Bicchi, A.: Shortest paths for finned, winged, legged, and wheeled vehicles with side-looking sensors. The International Journal of Robotics Research **31**(8), 997–1017 (2012)
19. Salaris, P., Cristofaro, A., Pallottino, L., Bicchi, A.: Shortest paths for wheeled robots with limited field-of-view: introducing the vertical constraint. In: Proceedings of the 52nd IEEE Conference on Decision and Control, pp. 5143 –5149 (2013)
20. Salaris, P., Cristofaro, A., Pallottino, L., Bicchi, A.: Epsilon–optimal synthesis for vehicles with vertically bounded field-of-view. IEEE Transactions on Automatic Control (in press)
21. Chitsaz, H., LaValle, S.M., Balkcom, D.J., Mason, M.: Minimum wheel-rotation for differential-drive mobile robots. The International Journal of Robotics Research pp. 66–80 (2009)
22. Balkcom, D., Mason, M.: Time-optimal trajectories for an omnidirectional vehicle. The International Journal of Robotics Research **25**(10), 985–999 (2006)
23. Souères, H., Laumond, J.P.: Shortest paths synthesis for a car-like robot. IEEE Transaction on Automatic Control pp. 672–688 (1996)
24. Sussmann, H., Tang, G.: Shortest paths for the Reeds-Shepp car: A worked out example of the use of geometric techniques in nonlinear optimal control. Tech. rep., Department of Mathematics, Rutgers University (1991)
25. Huifang, W., Yangzhou, C., Soueres, P.: A geometric algorithm to compute time-optimal trajectories for a bidirectional steered robot. Robotics, IEEE Transactions on **25**(2), 399–413 (2009)
26. Dubins, L.E.: On curves of minimal length with a constraint on average curvature, and with prescribed initial and terminal positions and tangents. American Journal of Mathematics pp. 457–516 (1957)
27. Cristofaro, A., Salaris, P., Pallottino, L., Giannoni, F., Bicchi, A.: On time-optimal trajectories for differential drive vehicles with field-of-view constraints. In: Proceedings of the 53rd IEEE Conference on Decision and Control (2014, in press)
28. Lou, H.: Existence and nonexistence results of an optimal control problem by using relaxed control. SIAM Journal on Control and Optimization **46**(6), 1923–1941 (2007)

29. Pedregal, P., Tiago, J.: Existence results for optimal control problems with some special nonlinear dependence on state and control. SIAM Journal on Control and Optimization **48**(2), 415–437 (2009)
30. Shiller, Z., Lu, H.: Computation of path constrained time optimal motions with dynamic singularities. Journal of dynamic systems, measurement, and control **114**(1), 34–40 (1992)
31. Hartley, R.I., Zisserman, A.: Multiple View Geometry in Computer Vision, second edn. Cambridge University Press, ISBN: 0521540518 (2004)
32. Salaris, P., Cristofaro, A., Pallottino, L.: Epsilon-optimal synthesis for nonholonomic vehicles with limited field-of-view sensors. Robotics, IEEE Transactions on **to appear** (2015)
33. Hartl, R.F., Sethi, S.P., Vickson, R.G.: A survey of the maximum principles for optimal control problems with state constraints. SIAM review **37**(2), 181–218 (1995)
34. Pontryagin, L.S.: Mathematical theory of optimal processes. CRC Press (1987)
35. Berkovitz, L.D., Medhin, N.G.: Nonlinear optimal control theory. CRC press (2012)
36. Bryson, A.E., Denham, W.F., Dreyfus, S.E.: Optimal programming problems with inequality constraints. AIAA journal **1**(11), 2544–2550 (1963)
37. Bryson, A., Ho, Y.: Applied optimal control. Wiley New York (1975)
38. Maurer, H.: On optimal control problems with bounded state variables and control appearing linearly. SIAM Journal on Control and Optimization **15**(3), 345–362 (1977)
39. Bonnard, B., Faubourg, L., Launay, G., Trélat, E.: Optimal control with state constraints and the space shuttle re-entry problem. Journal of Dynamical and Control Systems **9**(2), 155–199 (2003)
40. Clarke, F.: Functional analysis, calculus of variations and optimal control, vol. 264. Springer Science & Business Media (2013)
41. Johansen, T.A., Perez, T.: Unmanned aerial surveillance system for hazard collision avoidance in autonomous shipping. In: 2016 International Conference on Unmanned Aircraft Systems (ICUAS), pp. 1056–1065 (2016)
42. Sans-Muntadas, A., Pettersen, K.Y., Brekke, E.: Vision restricted path planning and control for underactuated vehicles. IFAC-PapersOnLine **49**(23), 199–206 (2016)

Appendix

8.1 Proof of Lemma 6.1

Lemma 8.1 *Let $\Psi(x)$ be the function defined in (30); then, for any $x, y > 0$ one has*

$$\Psi^{-1}(\Psi(x) + \Psi(y)) < \sqrt[3]{x^3 + y^3}.$$

Proof. Since $\Psi(\cdot)$ is an increasing function, we can consider the equivalent inequality

$$\Psi(x) + \Psi(y) < \Psi(\sqrt[3]{x^3 + y^3}).$$

Let us fix $y > 0$; we will prove that the function

$$h(x) = \Psi(x) + \Psi(y) - \Psi(\sqrt[3]{x^3 + y^3})$$

is negative for any $x > 0$. We have $h(0) = \Psi(y) - \Psi(\sqrt[3]{y^3}) = 0$ and

$$h'(x) = \Psi'(x) - \Psi'\left(\sqrt[3]{x^3 + y^3}\right) \frac{x^2}{(x^3 + y^3)^{\frac{2}{3}}}.$$

Now, by Taylor expansion, one has

$$\Psi(x) = \sum_{k=1}^{\infty} c_k x^{2k+1}, \quad c_k > 0 \ \forall k \in \mathbb{N}$$

and as a consequence

$$\Psi'(x) = \sum_{k=1}^{\infty} d_k x^{2k}, \quad d_k = (2k+1)c_k > 0 \ \forall k \in \mathbb{N}.$$

Using the latter equality in the expression of $h'(x)$ one gets

$$h'(x) = \sum_{k=1}^{\infty} d_k x^2 (x^{2k-2} - (x^3 + y^3)^{\frac{2k-2}{3}}) < 0$$

and the conclusion follows. □